Solar Sail Trajectory Analysis with Asymptotic Expansion Method

Lorenzo Niccolai, Alessandro A. Quarta*, Giovanni Mengali

Department of Civil and Industrial Engineering, University of Pisa, I-56122 Pisa, Italy

Abstract

An analytical expression for the trajectory equation of a solar sail spacecraft is available in special cases only, including the well known logarithmic spiral. The latter, however, cannot be used when the parking orbit is circular. This paper presents an approximate solution to this problem, obtained by considering the propulsive acceleration as a perturbation effect acting on a Keplerian trajectory in a heliocentric (two-dimensional) mission scenario. In this context, the spacecraft dynamics are approximated by an asymptotic series expansion in terms of non-singular generalized orbital elements. Under the assumption that the propulsive acceleration is small compared to the local Sun's gravitational attraction, a first order approximation is shown to be very accurate in predicting the trajectory of the spacecraft and the evolution of the non-singular orbital parameters of the osculating orbit. A periodic rectification procedure improves the method accuracy without significantly affecting the computational time, as is confirmed by numerical simulations.

Keywords: Solar sail analytical trajectory, Asymptotic expansion method, Mission analysis, Generalized orbital elements

Nomenclature

a	=	semimajor axis of osculating orbit, [au]
a_r, a_θ	=	radial and circumferential propulsive acceleration, [mm/s^2]
b_i	=	sail force coefficients
E	=	dimensionless auxiliary variable, see Eq. (47)
e	=	eccentricity of osculating orbit
h	=	angular momentum modulus, [au^2/day]
p	=	semilatus rectum of osculating orbit, [au]
q_i	=	generalized orbital elements
q_{ij}	=	j-th perturbation order term of q_i
R	=	dimensionless radial component of thrust
r	=	Sun-spacecraft distance, [au]
s	=	dimensionless auxiliary variable, see Eq. (7)
T	=	dimensionless circumferential component of thrust
t	=	time, [days]
v_r, v_θ	=	radial and circumferential velocity, [au/day]
α	=	sail cone angle, [deg]
β	=	lightness number
θ	=	angular coordinate, [deg]
$\mu_\odot$	=	Sun's gravitational parameter, [au^3/day^2]
ν	=	true anomaly on the osculating orbit, [deg]

*Corresponding author

Email addresses: lorenzo.niccolai@ing.unipi.it (Lorenzo Niccolai), a.quarta@ing.unipi.it (Alessandro A. Quarta), g.mengali@ing.unipi.it (Giovanni Mengali)

Published in Aerospace Science and Technology, online before print, June 2017. doi: https://doi.org/10.1016/j.ast.2017.05.038

σ = sail loading, $[\mathrm{g/m^2}]$
$\sigma^\star$ = critical sail loading, $[\mathrm{g/m^2}]$
ω = apse line rotation angle, [deg]

Subscripts

0 = initial
☿ = Mercury
r = point of rectification
s = numerical results

Superscripts

$\sim$ = dimensionless quantity
$-$ = post-rectification auxiliary variable, see Eqs. (51)–(52)

1. Introduction

The recent success of JAXA's IKAROS mission has demonstrated [1, 2, 3] the technological capability of deploying and actively controlling a photonic solar sail in the interplanetary space, thus opening revolutionary opportunities for new and advanced space missions that would be impossible to achieve with more conventional propulsion systems. Encouraged by these promising results and after the succeeding launch of NASA's NanoSail-D2 [4], other solar sail-based missions are still under development [5, 6].

Due to the low-thrust levels supplied by current generation solar sails, their effectiveness especially arises in extended-duration space missions. However, the mission analysis phase is a lengthy and difficult task, which is usually tackled by looking for the space trajectory that minimizes a scalar performance index, such as the mission time. This often implies the need of simulating a huge amount of possible "candidate" solutions, by numerically integrating the spacecraft equations of motion. In fact, an analytical form of the trajectory equation can be obtained in a few cases only. A well known example in this respect is obtained when the spacecraft orbital motion is two-dimensional, and the sail attitude (or the thrust angle) is maintained at a constant value with respect to a classical orbital reference frame [7, 8]. Under those assumptions, the trajectory polar equation coincides with a logarithmic spiral [9, 10, 11], which therefore represents an useful tool in the preliminary analysis of a solar sail-based mission [12]. There are, however, some intrinsic limitations to this solution. In fact, a logarithmic spiral trajectory cannot be used for the study of circle-to-circle orbital transfers [10] unless a discontinuity in the spacecraft inertial velocity is introduced both in the initial and final condition, that is, along the parking and target orbits. Some analytical (or semi-analytical) results not involving a logarithmic spiral-trajectory exist in the literature, such as the curve-fitting based formula for the flight time evaluation in an Earth-Mercury optimal rendezvous given by Dachwald [**?**]. These solutions can be effectively applied to specific cases (indeed, similar formulas can also be calculated and used for other mission scenarios), but their attainment requires the numerical analysis of a number of transfer trajectories.

The aim of this paper is to use a different approach in the analysis of solar sail heliocentric trajectories with a constant sail orientation. In the discussed approach, the propulsive acceleration is introduced in the equations of motion through a series expansion, assuming it is sufficiently small to be thought of as a perturbation term for the spacecraft (Keplerian) motion. The use of a series expansion to find an approximate solution for the trajectory equations has attracted some interest in the literature. In particular, starting from the theoretical work by Kevorkian [13], an interesting contribution to this subject may be found in Ref. [14], which uses a perturbational approximate approach to analyze the motion of a spacecraft propelled by a continuous low-thrust, whose modulus depends on the spacecraft distance from the primary. More recently, Bombardelli et al. [15] have characterized the motion of a spacecraft subjected to a continuous circumferential propulsive acceleration with an elegant series expansion method.

The results discussed in this paper make use of the three generalized orbital elements introduced in Ref. [15], and are obtained under the assumption of a heliocentric two-dimensional model and a fixed sail attitude (that is, a fixed cone angle). The proposed solution is validated by simulation, comparing the results with those achieved with a numerical integration of the equations of motions.

2. Solar sail equations of motion

Consider a spacecraft that initially tracks a heliocentric Keplerian parking orbit of eccentricity $e_0 < 1$ and semilatus rectum p_0. At time $t_0 \triangleq 0$, when the Sun-spacecraft distance is r_0 and the spacecraft true anomaly is $\nu_0 \in [0,\, 2\,\pi]$ rad, the primary propulsion system is switched on. The propulsive thrust is assumed to belong to the plane of the parking orbit for all $t \geq t_0$. The heliocentric spacecraft trajectory is therefore two-dimensional and, according to Bombardelli et al. [15], may be fully characterized by three non-singular (dimensionless) generalized orbital elements q_1, q_2, and q_3, defined as

$$q_1 \triangleq \frac{e}{\tilde{h}} \cos\omega \tag{1}$$

$$q_2 \triangleq \frac{e}{\tilde{h}} \sin\omega \tag{2}$$

$$q_3 \triangleq \frac{1}{\tilde{h}} \tag{3}$$

where e is the eccentricity of the osculating orbit, while ω is the angle between the eccentricity vector of the parking orbit $\boldsymbol{e}_0$ and that of the osculating orbit $\boldsymbol{e}$, see Fig. 1. In Eqs. (1)–(3), $\tilde{h}$ is the dimensionless modulus of the spacecraft angular momentum h, given by

$$\tilde{h} \triangleq \frac{h}{\sqrt{\mu_\odot\, r_0}} = \sqrt{\tilde{p}} \qquad \text{with} \qquad \tilde{p} \triangleq \frac{p}{r_0} \tag{4}$$

where $\mu_\odot$ is the Sun's gravitational parameter, and p the semilatus rectum of the osculating orbit.

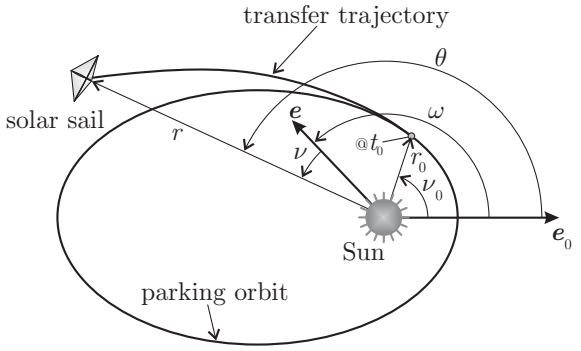

Figure 1: Geometrical sketch of the orbit transfer.

The differential equations describing the variation of the orbital elements with the spacecraft angular coordinate $\theta \triangleq \omega + \nu$ are [16]

$$\frac{\mathrm{d}}{\mathrm{d}\theta} \begin{bmatrix} q_1 \\ q_2 \\ q_3 \end{bmatrix} = \frac{1}{q_3 s^3} \begin{bmatrix} s\sin\theta & (s+q_3)\cos\theta \\ -s\cos\theta & (s+q_3)\sin\theta \\ 0 & -q_3 \end{bmatrix} \begin{bmatrix} \tilde{a}_r \\ \tilde{a}_\theta \end{bmatrix} \tag{5}$$

with

$$\tilde{a}_r \triangleq \frac{a_r}{\mu_\odot / r_0^2} \qquad \text{and} \qquad \tilde{a}_\theta \triangleq \frac{a_\theta}{\mu_\odot / r_0^2} \tag{6}$$

where a_r (or a_θ) is the radial (or circumferential) component of the propulsive acceleration, and s is an auxiliary variable defined as

$$s \triangleq q_1\, \cos\theta + q_2\, \sin\theta + q_3 \tag{7}$$

Using the main results of Ref. [15], the semimajor axis a, the eccentricity e, the Sun-spacecraft distance r, and the angle ω of the spacecraft osculating orbit can all be expressed as functions of the set $\{q_1, q_2, q_3, \theta, r_0\}$

as

$$a = \frac{r_0}{q_3^2 - q_1^2 - q_2^2} \tag{8}$$

$$e = \frac{\sqrt{q_1^2 + q_2^2}}{q_3} \tag{9}$$

$$r = \frac{r_0}{q_3^2 + q_1\, q_3\, \cos\theta + q_2\, q_3\, \sin\theta} \tag{10}$$

$$\omega = \arctan\left(\frac{q_2}{q_1}\right) \tag{11}$$

The dimensionless circumferential and radial components of the heliocentric spacecraft velocity are derived from the mechanical energy equation and the definition of the angular momentum, viz.

$$\tilde{v}_\theta \triangleq \frac{v_\theta}{\sqrt{\mu_\odot / r_0}} = q_1\, \cos\theta + q_2\, \sin\theta + q_3 \tag{12}$$

$$\tilde{v}_r \triangleq \frac{v_r}{\sqrt{\mu_\odot / r_0}} = q_1\, \sin\theta - q_2\, \cos\theta \tag{13}$$

Note that s coincides with $\tilde{v}_\theta$, see Eqs. (7) and (12). As such, s is different from zero with the exception of special trajectories in which the circumferential spacecraft velocity vanishes. Noteworthy situations in which $\tilde{v}_\theta$ may become equal to zero include the case of rectilinear orbits [17], trajectories with an angular momentum reversal maneuver [18], or trajectories for heliostationary missions [19]. All of these examples, however, require the use of high-performance solar sails, with a maximum propulsive acceleration on the order of (or even larger than) the local solar gravitational acceleration.

2.1. Solar sail thrust model

Consider a spacecraft propelled by a flat photonic solar sail with a classical optical force model [10, 20, 21]. The dimensionless propulsive acceleration components, see Eqs. (6), may be written in a compact form as

$$\tilde{a}_r = \beta\, \frac{R}{\tilde{r}^2} \qquad \text{and} \qquad \tilde{a}_\theta = \beta\, \frac{T}{\tilde{r}^2} \tag{14}$$

where $\tilde{r} = r/r_0$ is the dimensionless Sun-spacecraft distance with r given by Eq. (10), and β is the sail lightness number, defined as the ratio between the critical sail loading $\sigma^\star \triangleq 1.53\,\mathrm{g/m^2}$ to the actual sail loading σ [10]. Finally, the dimensionless variables R and T are given by

$$R = b_1\, \cos\alpha + b_2\, \cos^3\alpha + b_3\, \cos^2\alpha \tag{15}$$

$$T = b_2\, \cos^2\alpha \sin\alpha + b_3\, \cos\alpha \sin\alpha \tag{16}$$

where $\alpha \in [-\pi/2,\, \pi/2]$ rad is the sail cone angle, that is, the angle (positive when measured counterclockwise) from the Sun-spacecraft line to the normal to the sail reference plane in the direction opposite to the Sun, and $\{b_1, b_2, b_3\}$ are the force coefficients [21], whose values depend on the thermo-optical characteristics of the sail reflective film. For example, using the data taken from Wright [20] and McInnes [10] (corresponding to a square sail with a highly reflective aluminum coated front side and a highly emissive chromium-coated backside) the force coefficients are $b_1 = 0.0864$, $b_2 = 0.8272$, and $b_3 = -0.0055$. These data have been recently updated by Heaton and Artusio-Glimpse [22] (assuming a CP1 sail that is Al-coated on the front side and uncoated on the back side) to the new values $b_1 = 0.0723$, $b_2 = 0.8554$, and $b_3 = -0.0030$. Recall that in the ideal case of fully specular reflection of the impinging photons (i.e. for an ideal force model), the coefficients are $b_1 = b_3 = 0$ and $b_2 = 1$.

Substituting Eqs. (14) into Eqs. (5), the differential equations describing the spacecraft two-dimensional dynamics become

$$\frac{\mathrm{d}}{\mathrm{d}\theta}\begin{bmatrix} q_1 \\ q_2 \\ q_3 \end{bmatrix} = \beta\, q_3 \begin{bmatrix} \sin\theta & (1+q_3/s)\,\cos\theta \\ -\cos\theta & (1+q_3/s)\,\sin\theta \\ 0 & -q_3/s \end{bmatrix} \begin{bmatrix} R \\ T \end{bmatrix} \tag{17}$$

with initial conditions

$$q_1(\nu_0) = \frac{e_0}{\sqrt{1+e_0\,\cos\nu_0}} \tag{18}$$

$$q_2(\nu_0) = 0 \tag{19}$$

$$q_3(\nu_0) = \frac{1}{\sqrt{1+e_0\,\cos\nu_0}} \tag{20}$$

Note that at the initial time $t = t_0$, when the spacecraft tracks the parking orbit, $\omega = 0$ and $\theta = \nu_0$.

An interesting simplification of the previous differential equations is obtained if R and T remain constant along the spacecraft (propelled) trajectory. This happens when i) the thermo-optical characteristics of the reflecting film do not vary with time, which amounts to neglecting the degradation phenomenon of the sail material [23, 24], and ii) the cone angle α is held constant during the transfer. Notably, the case of motion with constant cone angle is particularly useful for different mission tasks, including a preliminary estimate of the optimal spacecraft trajectory [25, 26], the analysis of solar sail trajectories with low control authority [27], or the use of a shape-based approach for solar sail trajectory design [28].

However, even in the simplified case of R and T constant, the differential system of Eqs. (17) seems to not admit a closed form solution for a generic set of initial conditions. An exception is given by a Sun-facing sail, an arrangement that can be obtained passively using a suitable sail geometrical shape [29]. In that case the sail cone angle is zero along the whole trajectory, which implies $T \equiv 0$, see Eq. (16), and Eqs. (17)–(20) give

$$q_1 = \frac{e_0 + R\,\beta\,(\cos\nu_0 - \cos\theta)}{\sqrt{1+e_0\,\cos\nu_0}} \tag{21}$$

$$q_2 = \frac{R\,\beta\,(\sin\nu_0 - \sin\theta)}{\sqrt{1+e_0\,\cos\nu_0}} \tag{22}$$

$$q_3 = \frac{1}{\sqrt{1+e_0\,\cos\nu_0}} = \text{constant} \tag{23}$$

As a result, the semilatus rectum p (or, equivalently, the specific angular momentum modulus $\tilde{h}$) is a constant of motion, the trajectory is a conic and $\{a, e\}$ are periodic functions (with period 2π) of the angular coordinate θ, see Fig. 1.

In the general case when $\alpha \neq 0$ (which implies $T \neq 0$), an approximate but sufficiently accurate solution to the differential equations (17) may be found using an asymptotic expansion procedure in which the sail lightness number β is treated as a perturbation term, that is, the sail thrust is assumed to be a small disturbance acting on the spacecraft for a long time. This approximation is consistent with the current solar sail technological level since, for example, the sail lightness numbers of the Japanese solar sail demonstrator IKAROS [1] and the NASA's NanoSail-D2 [4] are $\beta = 0.001$ and $\beta = 0.003$, respectively.

3. Solution through series expansion

Paralleling the procedure discussed by Bombardelli et al. [15], the orbital elements $\{q_1, q_2, q_3\}$ defined in Eqs. (1)–(3) are now rewritten using a series expansion, in which the solar sail propulsive acceleration acts

as a perturbation term on the spacecraft Keplerian (reference) motion, viz.

$$q_1 = q_{10} + \beta\, q_{11} + O(\beta^2) \tag{24}$$

$$q_2 = q_{20} + \beta\, q_{21} + O(\beta^2) \tag{25}$$

$$q_3 = q_{30} + \beta\, q_{31} + O(\beta^2) \tag{26}$$

where q_{ij} are functions of the angular variable θ. In the previous equations, the subscript i denotes the orbital parameter ($i = 1, 2, 3$, see Eqs. (1)–(3)), whereas j represents the order of the perturbation term ($j = 0$ for unperturbed terms, $j = 1$ for first order terms).

Substituting Eqs. (24)–(26) into Eqs. (17) and equating the zeroth powers of β, the result is

$$\frac{\mathrm{d}q_{i0}}{\mathrm{d}\theta} = 0 \qquad \text{with} \qquad i = 1, 2, 3 \tag{27}$$

which amounts to stating that, as expected, the three generalized orbital elements are constant and the spacecraft tracks a Keplerian orbit when the perturbation effect by the propulsive acceleration is neglected. Enforcing the initial conditions on the parking orbit, the unperturbed values of the modified orbital elements are

$$q_{10} = q_1(\nu_0) \quad , \quad q_{20} = q_2(\nu_0) \quad , \quad q_{30} = q_3(\nu_0) \tag{28}$$

where $q_1(\nu_0)$, $q_2(\nu_0)$, and $q_3(\nu_0)$ are given by Eqs. (18)–(20).

An interesting result comes from the equations involving the first order powers of β. In fact, after some algebraic manipulations that are here neglected for the sake of conciseness, the first order perturbed dynamics equations can be written as

$$\frac{\mathrm{d}}{\mathrm{d}\theta}\begin{bmatrix} q_{11} \\ q_{21} \\ q_{31} \end{bmatrix} = \frac{\sqrt{1 + e_0\, \cos\nu_0}}{1 + e_0 \cos\theta} \begin{bmatrix} \sin\theta + e_0\, \sin\theta\, \cos\theta & 2\, \cos\theta + e_0\, \cos^2\theta \\ -\cos\theta - e_0\, \cos^2\theta & 2\, \sin\theta + e_0\, \sin\theta\, \cos\theta \\ 0 & -1 \end{bmatrix} \begin{bmatrix} R \\ T \end{bmatrix} \tag{29}$$

with the three initial conditions

$$q_{11}(\nu_0) = 0 \quad , \quad q_{21}(\nu_0) = 0 \quad , \quad q_{31}(\nu_0) = 0 \tag{30}$$

The solution to the initial value problem given by Eqs. (29)–(30) will now be discussed separately according to whether the parking orbit is circular or elliptical.

3.1. Circular parking orbit

When the parking orbit is circular ($e_0 = 0$), the initial conditions in Eqs. (18)–(20) become

$$q_1(\nu_0) \equiv q_2(\nu_0) = 0 \quad , \quad q_3(\nu_0) = 1 \tag{31}$$

Without loss of generality, due to the problem symmetry, assume $\nu_0 = 0$. The solutions to Eqs. (29)–(30) are

$$q_{11} = R\, (1 - \cos\theta) + 2\, T\, \sin\theta \tag{32}$$

$$q_{21} = -R\, \sin\theta + 2\, T\, (1 - \cos\theta) \tag{33}$$

$$q_{31} = -T\, \theta \tag{34}$$

The values of the non-singular orbital elements $\{q_1, q_2, q_3\}$ can be obtained by substituting Eqs. (28), and (31)–(34) into Eqs. (24)–(26). Neglecting the second order terms in the lightness number β, the (approximate) results for a circular parking orbit are

$$q_1 = R\, \beta\, (1 - \cos\theta) + 2\, T\, \beta\, \sin\theta \tag{35}$$

$$q_2 = -R\, \beta\, \sin\theta + 2\, T\, \beta\, (1 - \cos\theta) \tag{36}$$

$$q_3 = 1 - T\, \beta\, \theta \tag{37}$$

Notably, the previous solution is exact for a Sun-facing sail. In fact, as long as $T = 0$, Eqs. (35)–(37) coincide with Eqs. (21)–(23) when the condition $e_0 = 0$ is enforced.

The first order analytical approximation of the propelled trajectory equation, in polar form, is obtained from Eq. (10) as

$$r = \frac{r_0}{(1 - T\,\beta\,\theta)\,[1 + R\,\beta\,(\cos\theta - 1) + T\,\beta\,(2\sin\theta - \theta)]} \tag{38}$$

Likewise, using Eqs. (8)–(9), the semimajor axis and the eccentricity of the spacecraft osculating orbit are given by

$$a = \frac{r_0}{1 - 4\,\beta^2\,(R^2 + 4\,T^2)\,\sin^2(\theta/2) + T\,\beta\,\theta\,(T\,\beta\,\theta - 2)} \tag{39}$$

$$e = \frac{\beta\,\sqrt{2\,(R^2 + 4\,T^2)\,(1 - \cos\theta)}}{1 - T\,\beta\,\theta} \tag{40}$$

whereas, taking into account Eqs. (12)–(13), the circumferential and radial components of the spacecraft inertial velocity are

$$v_\theta = \sqrt{\frac{\mu_\odot}{r_0}}\,\left[1 - 2\,R\,\beta\sin^2(\theta/2) + T\beta\,(2\sin\theta - \theta)\right] \tag{41}$$

$$v_r = \sqrt{\frac{\mu_\odot}{r_0}}\,\left[2\,T\,\beta\,(1 - \cos\theta) + \beta\,R\,\sin\theta\right] \tag{42}$$

The expression for the eccentricity e of the osculating orbit, given by Eq. (40), provides a constraint on the maximum admissible value of θ that can be used in the approximation of the spacecraft trajectory. In fact, the condition $e \geq 0$ implies that

$$\theta \leq \frac{1}{T\,\beta} \quad \text{if} \quad T > 0 \tag{43}$$

In particular, for an ideal solar sail $T = \cos^2\alpha\sin\alpha$, see Eq. (16), which implies $\max(T) = 2\sqrt{3}/9$ and $\theta \leq 9/(2\beta\sqrt{3})$. However, in the special case when $T \to 0$ (i.e. for a Sun-facing solar sail), Eq. (43) states that no upper bound exists on the angular coordinate θ. This conclusion agrees with the fact that, as previously stated, the solution obtained via series expansion is exact.

3.2. Elliptic parking orbit

Consider now the more general case of an elliptic parking orbit, that is, $e_0 \in (0,\,1)$. It can be shown that the solutions of Eqs. (29)–(30) are

$$q_{11} = \frac{R\,(\cos\nu_0 - \cos\theta) + T\left(\sin\theta - \sin\nu_0 + \dfrac{\theta - \nu_0}{e_0} + \dfrac{E_0 - E}{e_0\,\sqrt{1 - e_0^2}}\right)}{\sqrt{1 + e_0\,\cos\nu_0}} \tag{44}$$

$$q_{21} = \frac{R\,(\sin\nu_0 - \sin\theta) + T\left[\cos\nu_0 - \cos\theta + \dfrac{1}{e_0}\,\ln\left(\dfrac{1 + e_0\cos\nu_0}{1 + e_0\cos\theta}\right)\right]}{\sqrt{1 + e_0\,\cos\nu_0}} \tag{45}$$

$$q_{31} = \frac{T\,(E_0 - E)}{\sqrt{(1 + e_0\,\cos\nu_0)\,(1 - e_0^2)}} \tag{46}$$

where E is an auxiliary variable [15] defined as

$$\tan\frac{E}{2} = \sqrt{\frac{1 - e_0}{1 + e_0}}\,\tan\frac{\theta}{2} \tag{47}$$

Substituting Eqs. (18)–(20) and (44)–(46) into Eqs. (24)–(26), and neglecting the second order terms in β, the approximate expressions for the three generalized orbital elements are

$$q_1 = \frac{e_0 + R\,\beta\,(\cos\nu_0 - \cos\theta) + T\,\beta\,\left(\sin\theta - \sin\nu_0 + \dfrac{\theta-\nu_0}{e_0} + \dfrac{E_0 - E}{e_0\,\sqrt{1-e_0^2}}\right)}{\sqrt{1 + e_0\,\cos\nu_0}} \tag{48}$$

$$q_2 = \frac{R\,\beta\,(\sin\nu_0 - \sin\theta) + T\,\beta\left[\cos\nu_0 - \cos\theta + \dfrac{1}{e_0}\,\ln\left(\dfrac{1+e_0\cos\nu_0}{1+e_0\cos\theta}\right)\right]}{\sqrt{1 + e_0\,\cos\nu_0}} \tag{49}$$

$$q_3 = \frac{\sqrt{1-e_0^2} + T\,\beta\,(E_0 - E)}{\sqrt{(1+e_0\,\cos\nu_0)\,(1-e_0^2)}} \tag{50}$$

Similar to what happens for a circular case, the previous equations give an exact result for a purely radial thrust ($T = 0$), see Eqs. (21)–(23). The polar equation of the trajectory $r(\theta)$ and the classical orbital elements of the osculating orbit, $a(\theta)$ and $e(\theta)$, can be obtained in an explicit form by substituting Eqs. (48)–(50) into Eqs. (8)–(10). However, their expressions are rather involved and are not reported here for conciseness.

3.3. Rectification procedure

Even though the results of the analytical method are in good agreement with numerical simulations for small values of θ, the error increases for large values of both the angular coordinate and the sail lightness number β. According to Ref. [15], a periodic rectification of the initial conditions of Eqs. (18)–(20) is useful for improving the result accuracy.

To this end, assume that the rectification is performed at a particular angular coordinate $\theta_r > \nu_0$, and introduce the following new variables

$$\bar{\theta} \triangleq \theta - \omega_r \quad , \quad \bar{\omega} \triangleq \omega - \omega_r \quad , \quad \bar{q}_1 \triangleq \frac{e}{\tilde{h}}\cos\bar{\omega} \quad , \quad \bar{q}_2 \triangleq \frac{e}{\tilde{h}}\sin\bar{\omega} \quad , \quad \bar{q}_3 \triangleq \frac{1}{\tilde{h}} \tag{51}$$

where the subscript r denotes a value taken just before the rectification instant. The initial conditions for the new variables are

$$\bar{\theta}_0 = \nu_r \quad , \quad \bar{\omega}_0 = 0 \quad , \quad \bar{q}_1\left(\bar{\theta}_0\right) = \frac{e_r}{\tilde{h}_r} \quad , \quad \bar{q}_2\left(\bar{\theta}_0\right) = 0 \quad , \quad \bar{q}_3\left(\bar{\theta}_0\right) = \frac{1}{\tilde{h}_r} \tag{52}$$

Note that Eqs. (44)–(46) can still be used to evaluate the first order perturbative effects on the $\bar{q}_i$ parameters, provided θ is substituted by $\bar{\theta}$. Moreover, it is important to highlight that rectifications increase the flexibility of the analytical method, since after a rectification the values of R and T in Eqs. (44)–(46) may be varied, to account for a (sudden) variation of the cone angle and/or a degradation of the sail film optical properties. In this sense, the rectification procedure can be used to simulate a piecewise constant steering law. The variation of $\{q_1, q_2, q_3\}$ with the angular coordinate θ is then obtained using a rotational matrix that aligns the eccentricity vector at the rectification point with the eccentricity vector on the parking orbit, viz.

$$\begin{bmatrix} q_1(\theta) \\ q_2(\theta) \\ q_3(\theta) \end{bmatrix} = \begin{bmatrix} \cos\omega_r & -\sin\omega_r & 0 \\ \sin\omega_r & \cos\omega_r & 0 \\ 0 & 0 & 1 \end{bmatrix} \begin{bmatrix} \bar{q}_1(\bar{\theta}) \\ \bar{q}_2(\bar{\theta}) \\ \bar{q}_3(\bar{\theta}) \end{bmatrix} \tag{53}$$

The rectification procedure can be repeated along the orbit to further reduce the difference between the analytical and the numerical simulation results, at the expense of an increase in computational time.

4. Model validation and verification

The proposed analytical method has been validated by comparing its results with the output of an orbital propagator (denoted with subscript s), which solves the spacecraft polar equations of motion in a

dimensionless form. The latter are numerically integrated in double precision using a variable order Adams-Bashforth-Moulton solver scheme [30, 31] with absolute and relative errors of 10^{-12}. To simplify the analysis, assume a perfectly reflecting ($b_1 = b_3 = 0$ and $b_2 = 1$) low-performance solar sail with $\beta \leq 0.0168$. Recall that, for an ideal force model, the sail lightness number may be related to the sail characteristic acceleration a_c through the relationship $a_c \simeq 5.93\,\beta$, where a_c, expressed in millimeters per second squared, is the maximum propulsive acceleration of the solar sail at a heliocentric distance of 1 au. Therefore, $\beta \leq 0.01686$ corresponds to a spacecraft characteristic acceleration $a_c \leq 0.1\,\mathrm{mm/s^2}$. Two different examples are now discussed, with a circular and an elliptic parking orbit.

4.1. Circular orbit case

Consider first the noteworthy case of a circular parking orbit ($e_0 = 0$) with radius $r_0 = 1\,\mathrm{au}$. This corresponds to a situation in which the solar sail-based spacecraft escapes from the Earth's gravitational field along a parabolic orbit relative to the starting planet.

The numerical simulations show that the proposed analytical method is able to accurately approximate the actual spacecraft heliocentric trajectory, with an error ϵ defined as

$$\epsilon \triangleq \max_{\theta} \left(\frac{|r_s(\theta) - r(\theta)|}{r_0} \right) \tag{54}$$

less than a few percentage points, provided the flight time Δt and the sail lightness number β (or a_c) are sufficiently small. This is confirmed by Fig. 2, which illustrates the simulation results for a time-span of two and four terrestrial years ($\Delta t = \{2, 4\}$ years) as a function of a fixed cone angle $\alpha \in [-90, 90]\,\mathrm{deg}$. More precisely, Fig. 2(a) shows the maximum modulus of the difference between the Sun-spacecraft distance $r_s(\theta)$ obtained by numerical integration of the equations of motion in the range $t \in [0, 2]$ years and that obtained with Eq. (38), the angular coordinate θ being the same. As expected, in the two special cases of radial thrust ($\alpha = 0$) and Keplerian motion ($\alpha = \pm 90\,\mathrm{deg}$) the analytical results coincide with the numerical ones, that is, $\epsilon = 0$. The error ϵ varies with the cone angle and the worst case approximately corresponds to $\alpha = \pm 35\,\mathrm{deg}$, when the modulus of the circumferential thrust T is maximum, see Eq. (16). However, even in the worst case of $|\alpha| = 35\,\mathrm{deg}$, the Sun-spacecraft distance calculated at $\Delta t = 2\,\mathrm{years}$ with Eq. (38) differs from the exact numerical value of less than about $0.007\,r_0$ only.

The error, of course, increases with the flight time Δt, as is confirmed by Fig. 2(b), which shows the numerical results obtained by doubling the flight time, i.e., assuming $\Delta t = 4\,\mathrm{years}$. However, even with such a long flight time, the error is rather small and does not exceed 3% of r_0. In particular, the maximum error is obtained at the end of the simulation, when θ takes its final (maximum) value, as is shown in the example of Fig. 3. The same figure also shows that the analytical results accurately approximate the values of the orbital elements (a and e) of the spacecraft osculating orbit.

The error ϵ may be further reduced using the previously described rectification procedure, at the price of an increase in computational time. To quantify this effect, consider a circular parking orbit with a radius $r_0 = 1\,\mathrm{au}$ and a flight time of $\Delta t = 4\,\mathrm{years}$. Figure 4 shows the results obtained when the trajectory is rectified 7 times, each one every six months. The error ϵ does not exceed about 8×10^{-3}, a value similar to that obtained with $\Delta t = 2\,\mathrm{years}$, but without any rectification procedure, see Fig. 2(a). In this example the rectification procedure increases the computational time of about a factor two.

The variation of the maximum error $\epsilon_{\max} \triangleq \max_{\alpha}(\epsilon)$ with the number of rectifications is illustrated in Fig. 5, assuming $a_c = 0.1\,\mathrm{mm/s^2}$, $\Delta t = 4\,\mathrm{years}$, and a parking orbit of radius $r_0 = 1\,\mathrm{au}$.

4.2. Elliptic orbit case

An example involving an elliptic orbit is obtained by simulating a simplified Earth-Mercury heliocentric transfer [32]. More precisely, the parking orbit of the solar sail-based spacecraft is taken as circular (with radius 1 au) and coplanar to the elliptic orbit of Mercury (with eccentricity $e_{\mathrm{☿}} = 0.2056$ and semimajor axis $a_{\mathrm{☿}} = 0.3871\,\mathrm{au}$). The solar sail is inserted into an escape trajectory (with respect to the Earth), coplanar to that of Mercury, with a hyperbolic excess speed v_∞. At the end of its interplanetary transfer the spacecraft performs a rendezvous with the target planet at its orbital aphelion. The solar sail characteristic acceleration of this example is $a_c = 0.1\,\mathrm{mm/s^2}$ and the cone angle (constant along the whole flight) is $\alpha = -35\,\mathrm{deg}$, in order to maximize the circumferential component of the propulsive acceleration.

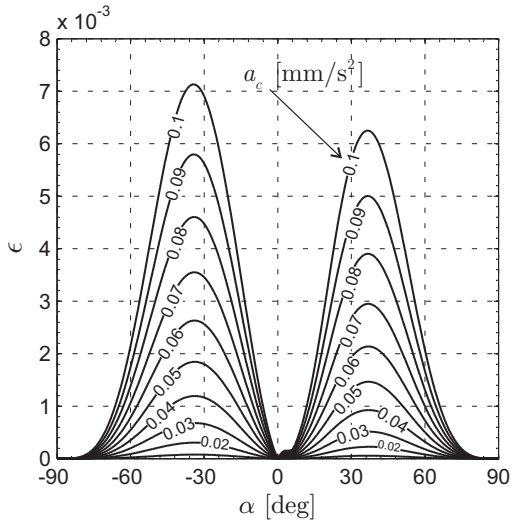

(a) Flight time $\Delta t = 2$ years.

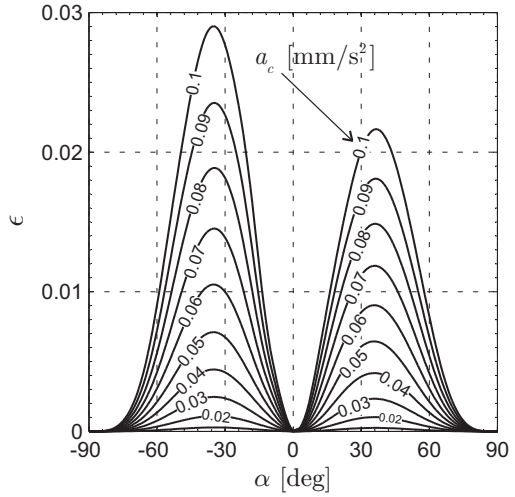

(b) Flight time $\Delta t = 4$ years.

Figure 2: Maximum errors of the analytical approximation as a function of α and a_c for a circular parking orbit with $r_0 = 1$ au.

The degree of approximation of the analytical approach can be quantified by simulation. To that end, let $\boldsymbol{r}_a$ and $\boldsymbol{v}_a$ denote the position and velocity vectors of a spacecraft that tracks the heliocentric Mercury's orbit when it crosses its aphelion. The actual solar sail trajectory has been calculated by a backward numerical integration of the spacecraft equations of motion, with initial conditions $\boldsymbol{r} = \boldsymbol{r}_a$ and $\boldsymbol{v} = \boldsymbol{v}_a$, until the solar sail reaches a distance of 1 au from the Sun, equal to the Sun-Earth distance along the circular parking orbit. The latter trajectory is shown in Fig. 6, where the black square marks the starting point of the heliocentric transfer, while the black circle denotes the rendezvous point. The hyperbolic excess speed $v_\infty \simeq 5.56\,\mathrm{km/s}$ is the modulus of the difference between the spacecraft velocity vector along the transfer trajectory when it crosses the parking orbit and the velocity vector along the (circular) parking orbit. During the transfer, the spacecraft completes about 9 full revolutions around the Sun, while the position vector sweeps out a total angle $\theta = 55.96\,\mathrm{rad}$.

A rough approximation of the transfer trajectory may be obtained using the analytical results given by Eqs. (48)–(50), with $\nu_0 = \pi\,\mathrm{rad}$ and $e_0 = e_{\mathrm{☿}}$, and considering a trajectory with a decreasing (negative) angular coordinate θ. The spacecraft position at the beginning of the transfer phase is characterized by the

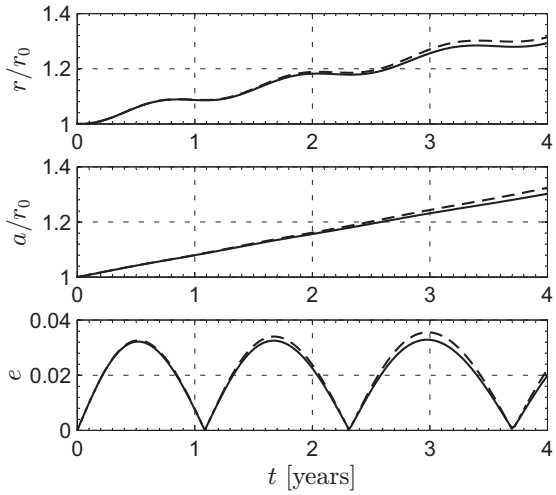

Figure 3: Comparison between analytical approximation (dashed line) and numerical results (solid line) when $a_c = 0.1$ mm/s^2 and $\alpha = 35$ deg.

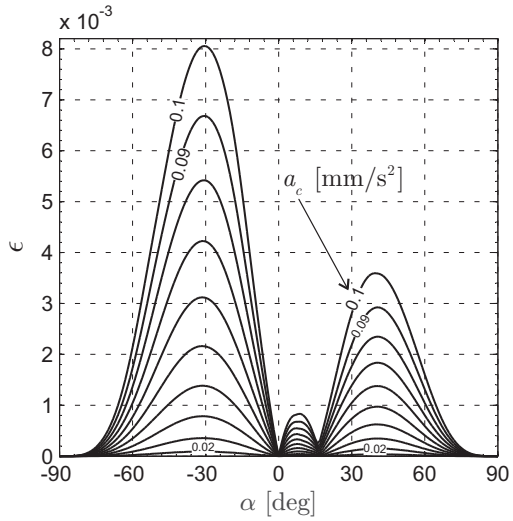

Figure 4: Value of the error ϵ with a flight time of $\Delta t = 4$ years and 7 rectifications.

angular coordinate $\theta = \theta_{\min}$, whose value is found by imposing the condition $r(\theta_{\min}) = 1$ au into Eq. (10). The hyperbolic excess speed is the modulus of the difference between the spacecraft velocity vector along the initial circular orbit and the velocity vector along the transfer trajectory in correspondence of $\theta_{\min}$, whose components are given by Eqs. (12)-(13). With this approach, the total angle swept out by the position vector is close to 50 rad (slightly less than 8 full revolutions around the Sun), see Fig. 7(a), and the hyperbolic excess speed is about 7 km/s. These values are quite different from those obtained by a numerical integration of the equations of motion. The error can be however substantially reduced with the rectification procedure. For example, using 10 rectifications, the total swept angle is 55.87 rad, the hyperbolic excess speed is 5.92 km/s and the transfer trajectory is now close to the real one, see Fig. 7(b). Figures 7(c) and 7(d) show the transfer trajectories obtained with 20 and 40 rectifications, respectively, and can be used to visualize the effect of the number of rectifications on the total error. In particular, the hyperbolic excess speed can be estimated with an error of a few meters per second only using 20 rectifications in the trajectory. Notably, even though the simulation time with 20 rectifications is about double than that necessary without any rectification, it is however very small (about 2% only) when compared to the time required to numerically integrate the

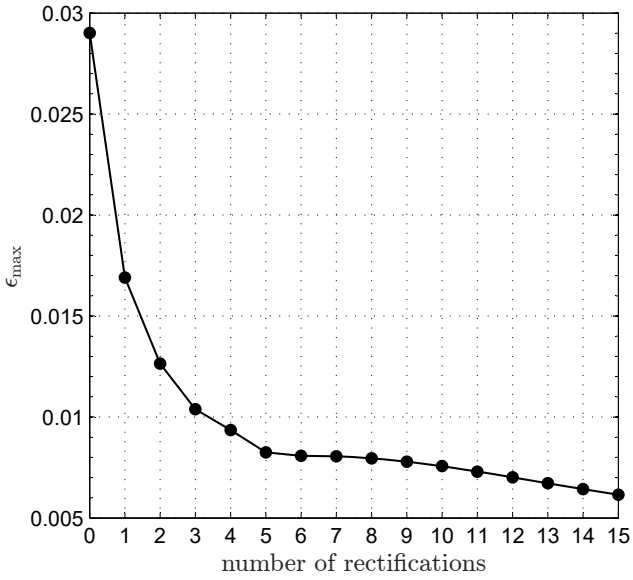

Figure 5: Maximum error $\epsilon_{\max}$ as a function of the number of rectifications with $a_c = 0.1$ mm/s^2 and $\Delta t = 4$ years.

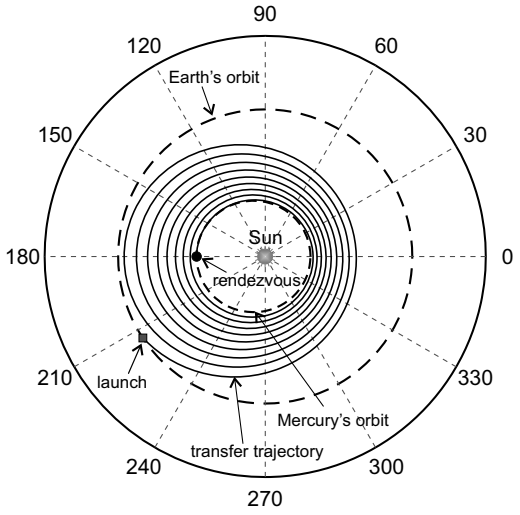

Figure 6: Earth-Mercury transfer trajectory evaluated through numerical simulation ($\alpha = -35$ deg, $a_c = 0.1$ mm/s^2, rendezvous at Mercury's aphelion).

equations of motion.

5. Mission applications

The previously discussed mathematical model is flexible enough to be successfully used for the study of different mission types. In particular, its effectiveness is now demonstrated in case of circular parking orbit.

To this end, consider a circle-to-circle heliocentric transfer. Let r_0 be the radius of the parking orbit and $r_f \neq r_0$ that of the final orbit. This example schematizes the heliocentric phase of an interplanetary transfer in which the actual eccentricity of the planetary orbits and their relative inclination are both neglected. Without loss of generality, let $\nu_0 = 0$ be the spacecraft initial true anomaly along the parking orbit and let

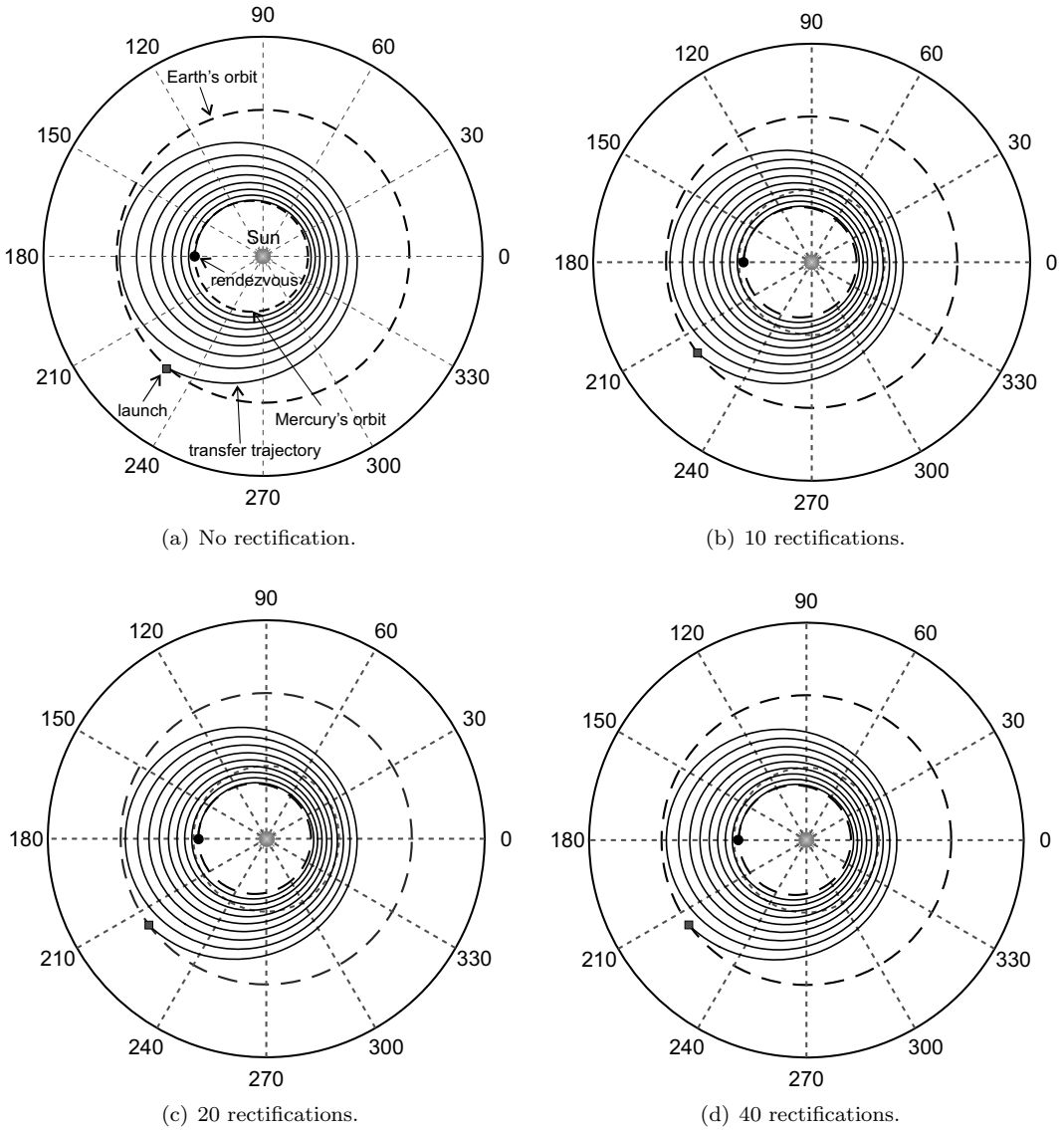

(a) No rectification.

(b) 10 rectifications.

(c) 20 rectifications.

(d) 40 rectifications.

Figure 7: Analytical approximation of the Earth-Mercury transfer trajectory ($\alpha = -35$ deg, $a_c = 0.1$ mm/s^2, rendezvous at Mercury's aphelion).

θ_f be its final true anomaly. The final conditions for the spacecraft are

$$r(\theta_f) = r_f \quad , \quad v_r(\theta_f) = 0 \quad , \quad v_\theta(\theta_f) = \sqrt{\mu_\odot / r_f} \tag{55}$$

The constant value of the sail cone angle ranges in the interval $\alpha \in (0, \pi/2)$ if $r_f > r_0$, or $\alpha \in (-\pi/2, 0)$ if $r_f < r_0$. The extreme values of the interval are to be excluded, otherwise the circle-to-circle transfer would be unfeasible. In fact, if $\alpha = \pm\pi/2$ the spacecraft has no thrust, while if $\alpha = 0$ it is subjected to a pure radial thrust that cannot change the spacecraft orbital angular momentum [33, 34].

Since the radial component of the spacecraft velocity at the end of the transfer is zero, Eq. (42) provides

$$\theta_f = k\, 2\, \pi \quad \text{with} \qquad k \in \mathbb{N}^+ \tag{56}$$

From this last equation, the analytical model for a circle-to-circle orbit transfer estimates the spacecraft to complete an integer number of revolutions (equal to k) around the Sun. This conclusion is in accordance

with the results discussed in Ref. [12] in which the circle-to-circle orbit transfer with a flat solar sail was analyzed within an optimal (i.e., minimum time) context with a cone angle that can be varied along the trajectory.

Substituting Eq. (56) into Eq. (41) and enforcing the last of Eqs. (55), the result is

$$\beta\, T = \frac{1 - \sqrt{r_0/r_f}}{2\, k\, \pi} \tag{57}$$

Since β is positive by definition, the sign of T (and so the sign of α) defines the mission type, that is, $T > 0$ implies an orbit raising ($r_0/r_f < 1$) while $T < 0$ defines an orbit lowering ($r_0/r_f > 1$). It may be verified that substituting Eqs. (56) and (57) into Eq. (38), the final distance is $r(\theta_f) = r_f$, that is, the first of Eqs. (55), is identically satisfied.

Equation (57) states that the circumferential thrust level T (and so the cone angle α) may be calculated as a function of the sail performance (in terms of lightness number β or characteristic acceleration a_c), the problem geometry (through the ratio r_0/r_f), and the number of revolutions k. Consider, for example, an Earth-Mars circle-to-circle orbit transfer in which $r_0 = 1\,\text{au}$ and $r_f = 1.523\,\text{au}$ and assume an ideal sail force model ($T = \sin\alpha\, \cos^2\alpha$). Figure 8 shows the isocontour lines of the function $a_c = a_c(\alpha, k)$, with $a_c \leq 0.1\,\text{mm/s}^2$. For a given number k of full revolutions, the minimum value of characteristic acceleration required for the transfer is obtained when $\alpha \cong 35\,\text{deg}$, which corresponds to the cone angle that maximizes the circumferential thrust for an ideal sail, see Eq. (16). The same figure also shows the presence of vertical asymptotes of the function $a_c = a_c(\alpha, k)$ when $\alpha \to \{0,\, \pi/2\}$, since in those cases the transfer cannot be carried out.

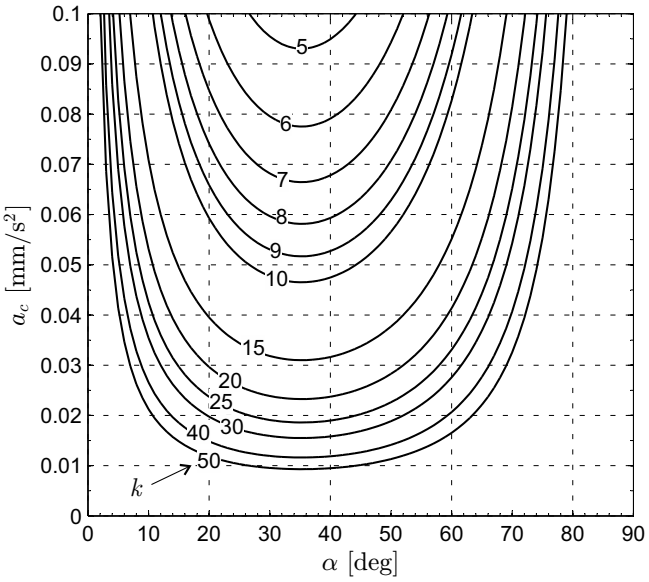

Figure 8: Characteristic acceleration as a function of the cone angle and number of revolutions in an Earth-Mars circle-to-circle orbit transfer for an ideal sail.

For example, in a Earth-Mars transfer ($r_0/r_f \simeq 0.6566$) with five full revolutions ($k = 5$) and a cone angle $\alpha = 35\,\text{deg}$, the required sail lightness number from Eq. (57) is $\beta \simeq 0.0157$ and the corresponding characteristic acceleration $a_c \simeq 0.093\,\text{mm/s}^2$ is approximately the minimum value along the isocontour line of Fig. 8. The trajectory obtained with the analytical approximation of Eq. (38) is compared, in Fig. 9(a), with the trajectory generated by forward integrating the equations of motion with $\alpha = 35\,\text{deg}$, until the final condition on the angular coordinate $\theta_f = 10\pi\,\text{rad}$ is met. The two trajectories are very similar even though the analytical approximation does not exactly satisfy the rendezvous conditions given by Eqs. (55), since $r(\theta_f)/r_f \simeq 0.962$, $v_r(\theta_f)/\sqrt{\mu_\odot/r_f} \simeq 10^{-3}$, and $v_\theta(\theta_f)/\sqrt{\mu_\odot/r_f} \simeq 1.02$. However, recall that the analytical model accuracy may be improved by rectifications.

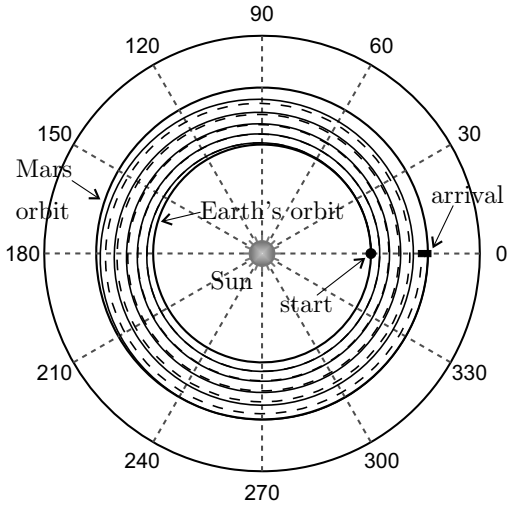

(a) Transfer trajectory.

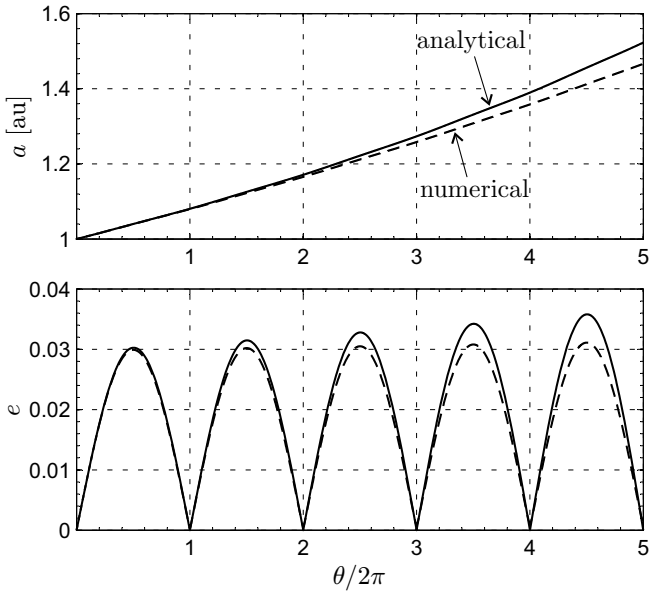

(b) Osculating orbit parameters.

Figure 9: Circle-to-circle Earth-Mars transfer with $k = 5$ and $\alpha = 35$ deg: analytical approximation (solid line) and numerical simulation (dashed line).

Consider now an Earth-Venus circle-to-circle transfer, in which $r_0 = 1\,\text{au}$ and $r_f = 0.723\,\text{au}$. The isocontour lines of the function $a_c = a_c(\alpha, k)$ are shown in Fig. 10, whose general appearance looks similar to that found in the Earth-Mars transfer, but with the difference that the cone angle is now negative (case of orbit lowering). For example, assuming $k = 5$ and a cone angle $\alpha = -35\,\text{deg}$, from Eq. (57) the lightness number is $\beta \simeq 0.0146$, which corresponds to a characteristic acceleration of $0.086\,\text{mm/s}^2$. The transfer trajectory and the time variation of the osculating orbital parameters are illustrated in Fig. 11. They are in good agreement with the results obtained by numerical integration of the equations of motion.

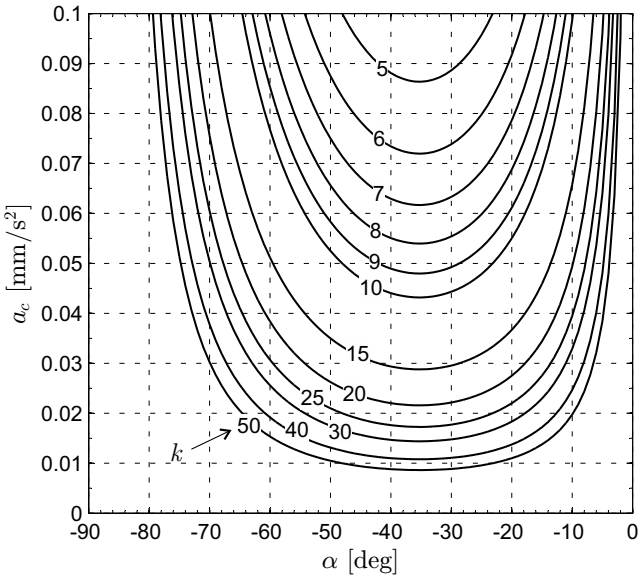

Figure 10: Characteristic acceleration as a function of the cone angle and number of revolutions in an Earth-Venus circle-to-circle orbit transfer for an ideal sail.

6. Conclusions

An analytical approximate solution for the two-dimensional equations of motion of a spacecraft propelled by a classical (flat) solar sail has been discussed. The results have been obtained under the assumption that the propulsive acceleration is small compared to the gravitational attraction, to such an extent that it may be considered as a perturbation effect. The spacecraft dynamics are described in terms of suitable non-singular orbital elements that are functions of an angular coordinate.

The proposed model is shown to be accurate as long as the sail lightness number is sufficiently small, as it happens in current solar sail-based missions. The accuracy of the results can be further increased with the introduction of a rectification procedure, which is periodically applied to the equations of motion to update their initial conditions. In addition, the sail attitude can be varied at every rectification point, thus simulating a steering law with a piecewise constant cone angle.

The proposed method guarantees a significant computational time saving, of about two order of magnitudes, when compared with a traditional approach in which the full equations of motion must be integrated numerically. This approach is therefore especially useful for direct optimization problems where a wide number of possible trajectories have to be investigated.

However, the analytical approximation currently requires the introduction of some simplifying assumptions that prevent the method from a general three-dimensional implementation. Future work will therefore try to circumvent such a restriction and focus on the possibility of accounting for a variable thrust, both in terms of modulus and direction.

Conflict of interest statement

The authors declared that they have no conflicts of interest to this work.

References

[1] Y. Tsuda, O. Mori, R. Funase, H. Sawada, T. Yamamoto, S. Takanao, T. Endo, K. Yonekura, H. Hoshino, J. Kawaguchi, Achievement of IKAROS - japanese deep space solar sail demonstration mission, in: 7th IAA Symposium on Realistic Advanced Scientific Space, Vol. 82, Aosta (Italy), 2011, pp. 183–188.

[2] O. Mori, Y. Tsuda, Y. Shirasawa, T. Saiki, Y. Mimasu, J. Kawaguchi, Attitude control of IKAROS solar sail spacecraft and its flight results, in: 61st International Astronautical Congress, Prague, Czech Republic, 2010, paper IAC-10.C1.4.3.

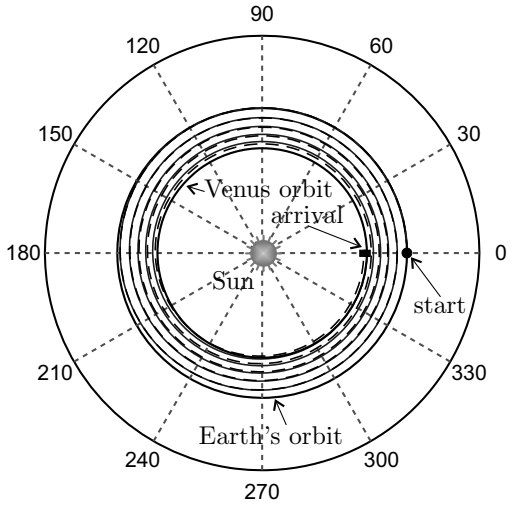

(a) Transfer trajectory.

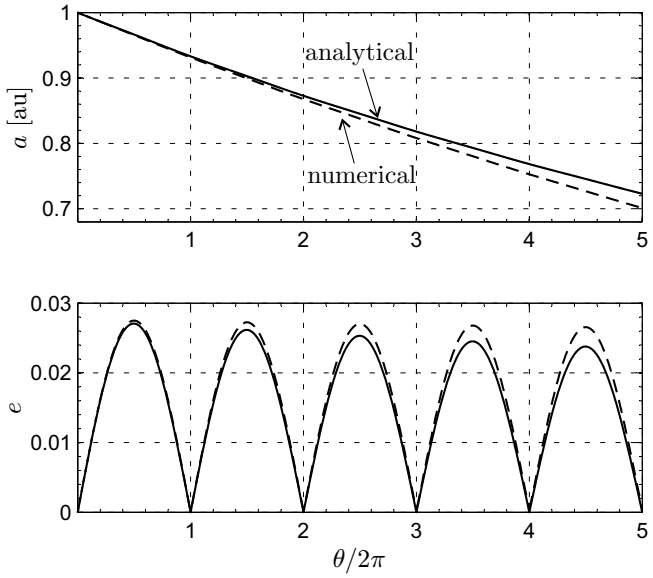

(b) Osculating orbit parameters.

Figure 11: Circle-to-circle Earth-Venus transfer with $k = 5$ and $\alpha = -35$ deg: analytical approximation (solid line) and numerical simulation (dashed line).

[3] R. Funase, Y. Shirasawa, Y. Mimasu, O. Mori, Y. Tsuda, T. Saiki, J. Kawaguchi, Fuel-free and oscillation-free attitude control of IKAROS solar sail spacecraft using reflectivity control device, in: 28th International Symposium on Space Technology and Science, Okinawa, Japan, 2011.

[4] L. Johnson, M. Whorton, A. Heaton, G. Laue, C. Adams, NanoSail-D: A solar sail demonstration mission, Acta Astronautica 68 (5–6) (2011) 571–575, doi: 10.1016/j.actaastro.2010.02.008.

[5] L. McNutt, L. Johnson, P. Kahn, J. Castillo-Rogez, A. Frick, Near-earth asteroid (NEA) scout, in: AIAA SPACE 2014 Conference and Exposition, San Diego (CA), 2014, paper AIAA 2014-4435.

[6] P. O. Hayne, B. T. Greenhagen, D. A. Paige, et al., Lunar flashlight: Illuminating the lunar south pole, in: 47th Lunar and Planetary Science Conference, The Woodlands (TX), 2016, paper 2761.

[7] A. E. Petropoulos, J. A. Sims, A review of some exact solutions to the planar equations of motion of a thrusting spacecraft, in: 2nd International Symposium Low Thrust Trajectories (LOTUS2), Toulouse (France), 2002.

[8] S. Wokes, P. Palmer, M. . Roberts, Classification of two-dimensional fixed-sun-angle solar sail trajectories, Journal of Guidance, Control, and Dynamics 31 (5) (2008) 1249–1258, doi: 10.2514/1.34466.

[9] R. H. Bacon, Logarithmic spiral: An ideal trajectory for the interplanetary vehicle with engines of low sustained thrust,

American Journal of Physics 27 (3) (1959) 164–165, doi: 10.1119/1.1934788.
[10] C. R. McInnes, Solar Sailing: Technology, Dynamics and Mission Applications, Springer-Praxis Series in Space Science and Technology, Springer-Verlag, Berlin, 1999, pp. 46–53, ISBN: 978-3-540-21062-7.
[11] J. Roa, J. Pelaez, J. Senent, New analytic solution with continuous thrust: Generalized logarithmic spirals, Journal of Guidance, Control, and Dynamics 39 (10) (2016) 2336–2351, doi: 10.2514/1.G000341.
[12] A. A. Quarta, G. Mengali, Semi-analytical method for the analysis of solar sail heliocentric orbit raising, Journal of Guidance, Control, and Dynamics 35 (1) (2012) 330–335, doi: 10.2514/1.55101.
[13] J. Kevorkian, The two-variable expansion procedure for the approximate solution of certain non-linear differential equations, Vol. 7, American Mathematical Society, 1966.
[14] W. Stavro, Low-thrust trajectories using the two variable asymptotic expansion method, Master's thesis, California Institute of Technology (1969).
[15] C. Bombardelli, G. Baù, J. Pelaez, Asymptotic solution for the two-body problem with constant tangential thrust acceleration, Celestial Mechanics and Dynamical Astronomy 110 (3) (2011) 239–256, doi: 10.1007/s10569-011-9353-3.
[16] J. Pelaez, J. Hedo, P. R. de Andrés, A special perturbation method in orbital dynamics, Celestial Mechanics and Dynamical Astronomy 97 (2) (2007) 131–150, doi: 10.1007/s10569-006-9056-3.
[17] A. A. Quarta, G. Mengali, Solar sail capabilities to reach elliptic rectilinear orbits, Journal of Guidance, Control, and Dynamics 34 (3) (2011) 923–926, doi: 10.2514/1.51638.
[18] G. Mengali, A. A. Quarta, D. Romagnoli, C. Circi, H2-reversal trajectory: a new mission application for high-performance solar sails, Advances in Space Research 48 (11) (2011) 1763–1777, doi: 10.1016/j.asr.2010.11.037.
[19] G. Mengali, A. A. Quarta, Optimal heliostationary missions of high-performance sailcraft, Acta Astronautica 60 (8-9) (2007) 676–683, doi: 10.1016/j.actaastro.2006.07.018.
[20] J. L. Wright, Space Sailing, Gordon and Breach Science Publishers, 1992, pp. 223–233.
[21] G. Mengali, A. A. Quarta, Optimal three-dimensional planetary rendezvous using non-ideal solar sail, Journal of Guidance, Control, and Dynamics 28 (1), doi: 10.2514/1.8325.
[22] A. F. Heaton, A. B. Artusio-Glimpse, An update to NASA reference solar sail thrust model, in: AIAA SPACE 2015 Conference and Exposition, Pasadena (CA), 2015, paper AIAA 2015-4506.
[23] B. Dachwald, M. Macdonald, C. R. McInnes, G. Mengali, A. A. Quarta, Impact of optical degradation on solar sail mission performance, Journal of Spacecraft and Rockets 44 (4) (2007) 740–749, doi: 10.2514/1.21432.
[24] B. Dachwald, G. Mengali, A. A. Quarta, M. Macdonald, Parametric model and optimal control of solar sails with optical degradation, Journal of Guidance, Control, and Dynamics 29 (5) (2006) 1170–1178, doi: 10.2514/1.20313.
[25] G. Mengali, A. A. Quarta, Optimal solar sail interplanetary trajectories with constant cone angle, in: M. Macdonald (Ed.), Advances in Solar Sailing, Springer Praxis Books, Springer Berlin Heidelberg, 2014, pp. 831–850.
[26] G. Mengali, A. A. Quarta, Solar sail trajectories with piecewise-constant steering laws, Aerospace Science and Technology 13 (8) (2009) 431–441, doi: 10.1016/j.ast.2009.06.007.
[27] J. Heiligers, G. Mingotti, C. R. McInnes, Optimal solar sail transfers between halo orbits of different sun-planet systems, Advances in Space Research 55 (5) (2015) 1405–1421, doi: 10.1016/j.asr.2014.11.033.
[28] A. Peloni, M. Ceriotti, B. Dachwald, Solar-sail trajectory design for a multiple near-earth-asteroid rendezvous mission, In press. Journal of Guidance, Control, and Dynamicsdoi: 10.2514/1.G000470.
[29] C. R. McInnes, Orbits in a generalized two-body problem, Journal of Guidance, Control, and Dynamics 26 (5) (2003) 743–749, doi: 10.2514/2.5129.
[30] L. F. Shampine, M. K. Gordon, Computer Solution of Ordinary Differential Equations: The Initial Value Problem, W. H. Freeman & Co Ltd, San Francisco, 1975, Ch. 10, ISBN: 0-716-70461-7.
[31] L. F. Shampine, M. W. Reichelt, The MATLAB ODE suite, SIAM Journal on Scientific Computing 18 (1) (1997) 1–22, doi: 10.1137/S1064827594276424.
[32] A. A. Quarta, G. Mengali, Solar sail missions to Mercury with Venus gravity assist, Acta Astronautica 65 (3–4) (2009) 495–506, doi: 10.1016/j.actaastro.2009.02.007.
[33] A. A. Quarta, G. Mengali, Analytical results for solar sail optimal missions with modulated radial thrust, Celestial Mechanics and Dynamical Astronomy 109 (2) (2011) 147–166, doi: 10.1007/s10569-010-9319-x.
[34] G. Mengali, A. A. Quarta, Heliocentric trajectory analysis of sun-pointing smart dust with electrochromic control, Advances in Space Research 57 (4) (2016) 991–1001, doi: 10.1016/j.asr.2015.12.017.